Journal of the Physical Society of Japan **83**, 044802 (2014)
http://dx.doi.org/10.7566/JPSJ.83.044802

Curvature Induced Discontinuous Transition for Semiflexible Biopolymers

Zicong Zhou*, Fang-ting Lin, Chin-yi Hung, Hao-Yun Wu, and Bo-Hen Chen

Department of Physics, Tamkang University, New Taipei City 25137, Taiwan, R.O.C.

(Received November 26, 2013; accepted February 3, 2014; published online March 26, 2014)

We study the effect of an intrinsic curvature on the mechanical property of two-dimensional semiflexible biopolymers and find that it can induce a discontinuous transition in extension. At zero temperature, we accurately show that the extension of an intrinsically curved semiflexible biopolymer of finite length can undergo a multiple-step discontinuous transition regardless of bending rigidity. The transition is accompanied by unwinding loops, and the critical force reaches a limit quickly with decreasing number of loops so that, in the experiment, it is possible to observe the almost simultaneous opening of several loops. However, the fluctuation or configurational average at a finite temperature suppresses the sharp transition so that there is no discontinuous transition in a system of finite size. However, our results obtained from Monte Carlo simulation reveal that, at a finite temperature, the extension of a biopolymer can undergo a one-step first-order transition in the thermodynamical limit if the biopolymer has a sufficiently large bending rigidity. The critical force increases with increasing intrinsic curvature or bending rigidity.

1. Introduction

The mechanical property of semiflexible biopolymers has attracted considerable attention owing to its importance in understanding the structure and function of biological materials. For instance, it is crucial to determine the roles of actin and actin homolog proteins in the regulation of cell shape and the organization of the cytoskeleton in cells. Moreover, the mechanical property also affects how double-stranded DNA (dsDNA) wraps around histones and is packed into phage heads. It is well known that a wormlike chain (WLC) model clearly describes the entropic elasticity of intrinsically straight semiflexible biopolymers.[1–3] In the WLC model, a chain extends smoothly with increasing applied force so that no phase transition occurs. It is also clear that adding a nonvanishing intrinsic torsion alone to the WLC model cannot change the smooth variation in the extension if we do not fix the initial tilting angle and cross section of the chain, i.e., if we adopt a hinged boundary condition (BC). In contrast, it has been reported that an intrinsically curved and twisted biopolymer can form a stable helix, and that the extension of a helix can undergo a discontinuous transition even without considering the effect of temperature (T).[4–9] One can then ask whether a nonvanishing intrinsic curvature alone is enough to induce a discontinuous transition. Intrinsically curved biopolymers are common occurrence in nature. For instance, for short dsDNA chains, special sequence orders favor a finite intrinsic curvature.[10–13] A good example is that tandem sequence repeats of adenine tracts (A-tracts) can yield a constant intrinsic curvature in dsDNA.[11,12] It has also been reported that, with a long-range correlation in sequence, dsDNA develops a macroscopic (intrinsic) curvature so that the WLC model fails to account for its property.[14] Therefore, the mechanical property of an intrinsically curved semiflexible biopolymer is a significant topic. Moreover, many experiments on semiflexible biopolymers have been performed in a two-dimensional (2D) environment so that the property of biopolymers in 2D has attracted growing interest.[14–24] Therefore, for simplicity, we focus on the 2D system in this work. In this study, we accurately show that, at $T = 0$, the extension of an intrinsically curved biopolymer can undergo a multiple-step discontinuous transition even with a finite length, regardless of bending rigidity. In contrast, we find that a finite T results in considerable changes and that a sharp transition occurs only in the thermodynamical limit if the biopolymer has a sufficiently large bending rigidity.

The paper is organized as follows. In Sect. 2, we describe our model. In Sect. 3, we present the accurate calculations for multiple-step discontinuous changes in extension at zero temperature. In Sect. 4, we focus on the sharp transition of extension at a finite temperature. The main text ends with conclusions and a discussion. Finally, we present some mathematical details in Appendix.

2. Model

2.1 Continuous model

A semiflexible biopolymer is often modeled as a filament. In a 2D case, the configuration of a filament is determined by a vector, $\mathbf{t} \equiv d\mathbf{r}/ds = \{\cos\phi, \sin\phi\}$, which is tangent to the contour line of the filament, where $\mathbf{r} = (x, y)$ is the locus of the filament, s is the arc length, and $\phi(s)$ is the angle between the x-axis and $\mathbf{t}$, as shown in Fig. 1(a). One end of the chain (at $s = 0$) is fixed at $x = 0$. Applying a uniaxial force (along the x-axis) F_x to another end at $s = L$, we can write the elastic energy of an intrinsically curved filament as[14–16]

$$E_L = \frac{k}{2}\int_0^L ds(\dot{\phi} - \tilde{c})^2 - F_x x_L = \frac{k}{2}\int_0^L ds(\dot{\phi} - \tilde{c})^2 - F_x \int_0^L \cos\phi\, ds, \quad (1)$$

where k is the bending rigidity, L is the contour length as well as a constant so that the filament is inextensible, $\dot{\phi} \equiv \dot{x}\ddot{y} - \dot{y}\ddot{x}$ is the signed curvature, $\tilde{c}$ is the intrinsic signed curvature, and $x_L \equiv x(L)$ is the extension. $\tilde{c} \neq 0$ means that, when $F_x = 0$, the ground-state configuration (GSC, or the spontaneous configuration, i.e., the configuration with the lowest energy) of the filament is a curve of curvature $\tilde{c}$. The symbol "$\cdot$" represents the derivative with respect to s. $\tilde{c}$ can be s-dependent, but for simplicity, in this work, we consider only an s-independent or constant $\tilde{c}$. $\tilde{c}$ can also be either positive or negative, but without loss of generality we assume $\tilde{c} > 0$ and $F_x > 0$. When $\tilde{c} = 0$, it is reduced to the WLC model.

2.2 Discrete model

The force-extension relationship of the continuous model

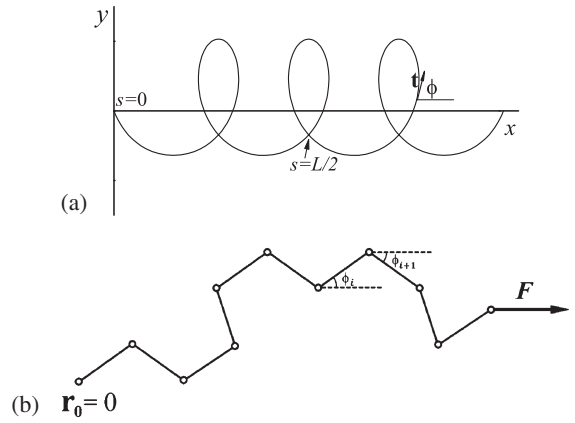

Fig. 1. (a) Schematic diagram of a filament showing the notation used. (b) Schematic diagram of the discrete model.

at a finite T and under a low or very strong force has been studied.[16] However, the mechanical property of the system under a moderate force and at a finite T is yet elusive. To solve this problem, we discretize the model and perform Monte Carlo simulation with the Metropolis algorithm to study it. In the discrete model, a filament consists of N straight segments of length l_0 joined end to end, as shown in Fig. 1(b). The coordinates of the two ends of the i-th segment are therefore $\{x_{i-1}, y_{i-1}\}$ and $\{x_i, y_i\}$ with $x_0 = y_0 = 0$. By replacing $\dot{\phi}$ with $(\phi_{i+1} - \phi_i)/l_0$ and introducing the reduced energy, $\mathcal{E}_N$, the elastic energy becomes

$$\mathcal{E}_N \equiv \frac{E_N}{k_B T} = \frac{\kappa}{2}\sum_{i=1}^{N-1}(\phi_{i+1} - \phi_i - c)^2 - f\sum_{i=1}^{N}\cos\phi_i, \qquad (2)$$

where k_B is the Boltzmann constant, $c \equiv \tilde{c} l_0$, $\kappa \equiv k/l_0 k_B T$, and $f \equiv F_x l_0/k_B T$. We also scale the length by l_0 so $x_N = \sum_{i=1}^{N}\cos\phi_i$ and define the relative extension as $z_N = \langle x_N\rangle/N$, where $\langle\cdots\rangle$ denotes the configurational or thermal average.

3. Multiple-Step Discontinuous Changes in Extension at Zero Temperature

3.1 General expressions

Extremizing E_L, we obtain the shape equation and BC that governs the configuration of the filament in the ground state,[16]

$$k\ddot{\phi} - F_x \sin\phi = 0, \qquad (3)$$

$$\dot{\phi}_0 - \tilde{c} = \dot{\phi}_L - \tilde{c} = 0, \qquad (4)$$

where $\phi_0 = \phi(0)$ and $\phi_L = \phi(L)$. Equation (4) means that both ϕ_0 and ϕ_L are not fixed, i.e., it gives hinged BC. We do not consider other forms of BC in this work since for a long filament, the form of BC is in fact irrelevant.

For a short ($L < 2\pi/\tilde{c}$) filament the solution of Eq. (3) has been studied analytically.[16] In this work we extend it to a more general case with $L > 2\pi/\tilde{c}$. The essential difference between short and long filaments is that a long one can form loops, as shown in Fig. 1(a), but a short one cannot.

From Eq. (3), we find (see Appendix)

$$L = \frac{2n}{\tilde{c}}\int_0^{\pi}\frac{d\phi}{\sqrt{1 + F(\cos\phi'_L - \cos\phi)}} + \frac{2}{\tilde{c}}\int_0^{\phi'_L}\frac{d\phi}{\sqrt{1 + F(\cos\phi'_L - \cos\phi)}}, \qquad (5)$$

$$x_L = \frac{2n}{\tilde{c}}\int_0^{\pi}\frac{\cos\phi\, d\phi}{\sqrt{1 + F(\cos\phi'_L - \cos\phi)}} + \frac{2}{\tilde{c}}\int_0^{\phi'_L}\frac{\cos\phi\, d\phi}{\sqrt{1 + F(\cos\phi'_L - \cos\phi)}}, \qquad (6)$$

$$\mathcal{E}_L = n\int_0^{\pi}\sqrt{1 + F(\cos\phi'_L - \cos\phi)}\, d\phi + \int_0^{\phi'_L}\sqrt{1 + F(\cos\phi'_L - \cos\phi)}\, d\phi - 2(n\pi + \phi'_L) - \tilde{c}F x_L/2, \qquad (7)$$

where $F \equiv 2F_x/(k\tilde{c}^2)$, $\mathcal{E}_L \equiv E_L/k\tilde{c}$ is the reduced energy, n is the number of loops, $\phi'_L = \phi_L - 2n\pi = -\phi_0$, and $\pi \geq \phi'_L > 0$. It is clear that, when $F = 0$, $n = n_0 \equiv \mathrm{Int}(L\tilde{c}/2\pi)$, where $\mathrm{Int}(X)$ gives the integer part of X. It is also clear that $n \leq n_0$ for a stable state. ϕ_L is dependent on L, n, and F; x_L is dependent on ϕ_L, n, and F. With L and F given, we can find $\phi_L(L)$ from Eq. (5) and substitute it into Eqs. (6) and (7) to find x_L and $\mathcal{E}_L$, respectively. For convenience, at $T = 0$, we scale the length by $1/\tilde{c}$ so that L and x_L are dependent on $\tilde{c}$ implicitly, whereas $\mathcal{E}_L$ is dependent on $\tilde{c}$ explicitly.

3.2 Multiple-step discontinuous changes in extension for a long filament

The force-extension relationship of a short filament ($n_0 = 0$) was studied and no phase transition was found.[16] However, in this work, we find that, when $n_0 \geq 1$, the result is completely different. Intuitionally, this is because, if the number of loops is unchanged, increasing F will increase the $\dot{\phi}$ of loops and the bending energy markedly, so that unwinding loops can lower energy markedly at a strong force.

We first note that x_L and L diverge when and only when $\cos\phi'_L = 1 - 1/F$. More exactly, $L \to -\log 0^+ \to \infty$ and $x_L \to -\log 0^+ \to \infty$ when $\cos\phi'_L \to 1 - 1/F$. This is because in this case, near $\phi = 0^+$, $1 + F(\cos\phi'_L - \cos\phi) \approx F\phi^2/2$. It follows that, at a large F and a large L, $\cos\phi'_L \approx 1 - 1/F$ and $\phi'_L \to 0$ when $F \to \infty$. In other words, at a large force, the filament is close to a straight line since $n = 0$ and $\phi'_L = \phi_L \geq \phi \geq 0$ in integration, in agreement with our daily life experience.

In the continuous model, we define the relative extension as $z_L = x_L/L$. Note that, when $L\tilde{c}/2\pi$ is not an integer, $z_L \neq 0$ at $F = 0$. This is quite different from that at a finite temperature because we do not need to perform configurational averaging at $T = 0$. Evaluating Eqs. (5)–(7) numerically, we obtain four important conclusions as follows.

Firstly, at a given L, in general, ϕ_L, x_L, and $\mathcal{E}_L$ obtained from Eqs. (5)–(7) are multiple-value functions of F, and we can use n to denote different branches of each function. When $F < 0.5$, the number of branches is dependent on F. This is because, in this case, $1 + F(\cos\phi'_L - \cos\phi) > 1 - 2F$, so from Eq. (5) we know that $L < 2\phi_L/\tilde{c}\sqrt{1 - 2F}$. This suggests that, when F is smaller than a bound ($\equiv F_0 < 0.5$), a large L requires a large ϕ_L, or n cannot be much smaller than n_0, otherwise there would be no solution to Eq. (5). For instance, when $L = 21\pi/\tilde{c}$, we find that Eq. (5) has no real solution to ϕ_L at a low F if $n < 9$, as shown in Fig. 2(a). F_0 is dependent on n, and the larger the n, the smaller the F_0. For example, with $L = 21\pi/\tilde{c}$, we obtain $F_0 = 0.237$ when

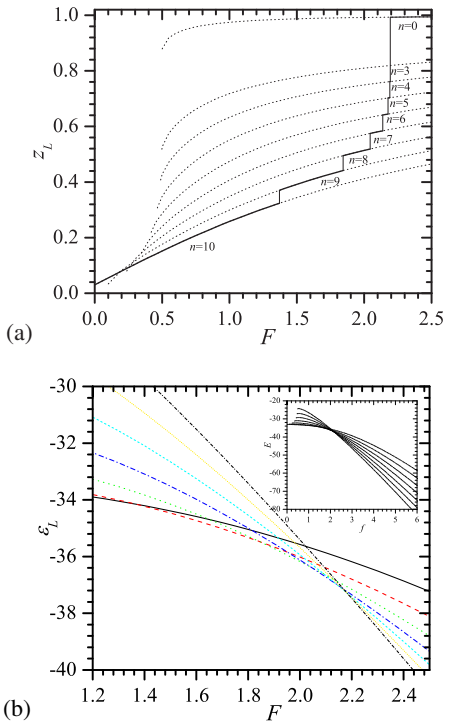

Fig. 2. (Color online) (a) The dashed lines represent different branches of z_L vs F for a filament with $L = 21\pi/\tilde{c}$ ($n_0 = 10$) and $\tilde{c} = 0.5$. The solid line represents the most possible path observed in the experiment. The vertical solid lines correspond to F_n. (b) Different branches of $\mathcal{E}_L$ vs F for a filament with $L = 21\pi/\tilde{c}$ and $\tilde{c} = 0.5$. $n = 10$ (solid black), 9 (red dashed), 8 (green dotted), 7 (blue dash-dotted), 6 (cyan short-dashed), 5 (yellow short-dotted), and 4 (black short-dash-dotted). Reduced units are used.

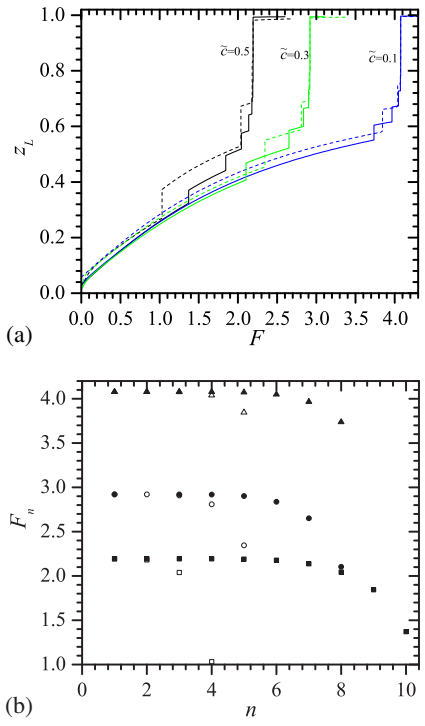

Fig. 3. (Color online) (a) Most possible z_L vs F for filaments with $\tilde{c} = 0.5$, $L = 8.2\pi/\tilde{c}$ (black dashed) and $L = 21\pi/\tilde{c}$ (black solid); $\tilde{c} = 0.3$, $L = 16.2\pi/\tilde{c}$ (green solid) and $L = 10.6\pi/\tilde{c}$ (green dashed); $\tilde{c} = 0.1$, $L = 16.6\pi/\tilde{c}$ (blue solid) and $L = 11.0\pi/\tilde{c}$ (blue dashed). (b) F_n vs n for filaments with $\tilde{c} = 0.5$, $L = 8.2\pi/\tilde{c}$ (open square) and $L = 21\pi/\tilde{c}$ (filled square); $\tilde{c} = 0.3$, $L = 16.2\pi/\tilde{c}$ (filled circle) and $L = 10.6\pi/\tilde{c}$ (open circle); $\tilde{c} = 0.1$, $L = 16.6\pi/\tilde{c}$ (filled triangle) and $L = 11.0\pi/\tilde{c}$ (open triangle). Reduced units are used.

$n = 8$, but $F_0 = 0.4979$ when $n = 3$, as shown in Fig. 2(a). In contrast, when $F > F_0$, we can find a solution to Eq. (5) at any $n \leq n_0$, so that, at a large F (≥ 0.5), ϕ_L, x_L, and $\mathcal{E}_L$ are always multiple-value functions of F, the number of branches of each function is equal to n_0, and different n values give different branches, as shown in Fig. 2(a). Moreover, from Fig. 2(a), we can also see that, when F is large, there is no crossover between the different branches of z_L.

Secondly, at the same L and $\tilde{c}$, the different branches of the energy curve (i.e., the relationship between $\mathcal{E}_L$ and F) always intersect, resulting in a transition in z_L with varying F. The transition is associated with unwinding loops. With the same L and $\tilde{c}$, we find that at a low F, the state with a larger n has a lower energy. But, at a large F, the state with a smaller n has a lower energy. Therefore, at the given L and $\tilde{c}$, the different branches of $\mathcal{E}_L(F)$ always intersect at some forces, as shown in Fig. 2(b) for a typical example. This means that we cannot observe every branch of $z_L(F)$ [dotted lines in Fig. 2(a)] in the experiment since they cannot all be in the lowest energy state (i.e., the ground state). It follows exactly that the observable z_L is a piecewise function of F combined with pieces in different branches, and shifts from one branch to another at the crossover of the energy curve. Moreover, with varying F, the energy curves with the nearest n always intersect first. It follows that, with increasing F, the most possible relation between z_L and F shifts from the nth branch to the $(n-1)$th branch successively at a critical force F_n, as shown in Figs. 2(a) and 3(a), in which an abrupt transition (denoted by the vertical lines) occurs at F_n. Therefore, with increasing F, the most possible $z_L(F)$ goes from one branch to another, unwinding one loop at a time instead of opening several loops simultaneously. Our calculations further show that the larger the $\tilde{c}$, the smaller the F_n, as shown in Fig. 3. However, since $F = 2F_x/(k\tilde{c}^2)$, exactly the real critical force is still smaller for a smaller $\tilde{c}$.

Thirdly, F_n tends to a limit quickly with decreasing n, as shown in Figs. 2(a) and 3. The limit of F_n is clearly dependent on $\tilde{c}$. The larger the $\tilde{c}$, the larger the limit. For instance, when $L = 21\pi/\tilde{c}$ and $\tilde{c} = 0.5$, $F_2 \approx F_3 \approx 2.193$ is numerically indistinguishable, as shown in Figs. 2(a) and 3(a). This limit is almost independent of L. Therefore, it is possible to open several loops all at once in the experiment and it can give more than 30% jumps in z_L, as shown in Figs. 2(a) and 3.

Fourthly, opening a loop is always accompanied by a discontinuous change in x_L, but the energy is still continuous, as we can see from Figs. 2, 3(a), and 4(b). From Fig. 4(a), we also see that ϕ'_L tends to $\arccos(1 - 1/F)$ rapidly with decreasing n. Figure 4(b) shows some configurations just before and after transition. From Fig. 4(b), we find that there is hardly a change in the shape of the loop, providing another evidence that the change in extension is indeed dominated by unwinding loops.

Our calculations also show that $\mathcal{E}_L(F)$ with a given n intersects with all other branches with the same L and $\tilde{c}$, as shown in Fig. 2(b) for a typical example. This indicates that, in the experiment, the jump may occur at some forces other than F_n, if the rate of increasing or decreasing force is too

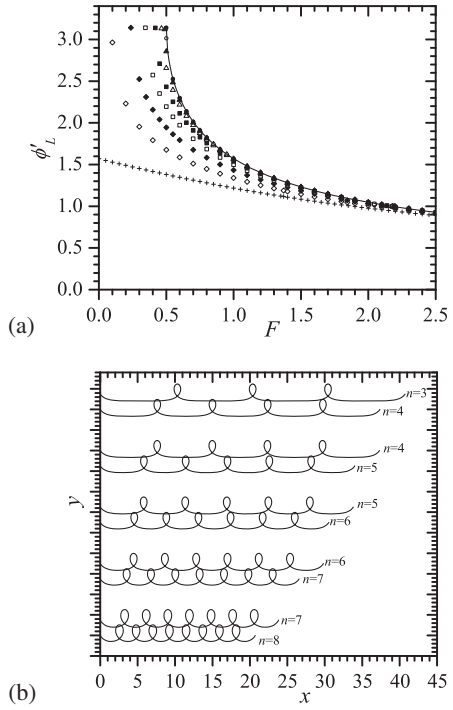

Fig. 4. (a) Different branches of ϕ'_L vs F for a filament with $\tilde{c} = 0.5$ and $L = 10.6\pi/\tilde{c}$. From bottom to top, $n = 10$ (plus), 9 (open diamond), 8 (filled diamond), 7 (open square), 6 (filled square), 5 (open triangle), 4 (filled triangle), 3 (open circle), and 1 (filled circle). The top solid line is given by $\cos\phi'_L = 1 - 1/F$. (b) Critical configurations of a filament with $\tilde{c} = 0.3$ and $L = 16.2\pi/\tilde{c}$. The y-coordinates are shifted for clarify. Reduced units are used.

fast. The existence of multiple crossovers and F_0 therefore reveals the possibility of observing hysteresis in the experiment. The discontinuous transition in z_L and possible hysteresis suggest that the extension of a long filament undergo a typical multiple-step first-order transition at an arbitrary k and a finite L.

Finally, note that all conclusions in this section are also valid for a 3D filament. This is because, owing to symmetry, with hinged BC and under a uniaxial force, the GSC of a 3D filament must also lie in a plane, and so the results are the same as those of the 2D system. We should also point out that this conclusion is valid only for a twist-free filament.

4. Abrupt Transition at Finite Temperature

In the last section, we find a multiple-step discontinuous transition at $T = 0$ for an arbitrary k and a large but finite L. The transition results from the existence of multiple solutions in the shape equation for given L, F, and $\tilde{c}$, but the ground state must have the lowest energy so that it is unique. At a finite temperature, we need to average all possible configurations, and intuitionally such an average will smoothen the change, especially if the jump in z_L is small and $F_n - F_{n-1}$ is large. Therefore, whether the transition still exists at a finite temperature is an intriguing question. From the results in Sect. 3.2, we know that the last step of transition opens several loops almost simultaneously, resulting in more than 30% changes in z_L, so we expect that the transition will also occur at a finite T, at least when the bending rigidity is sufficient large.

In our simulation, most of the initial configurations are set randomly. We also set the initial configuration as a circle of curvature c for a few samples but find no difference. We equilibrate every sample from 5×10^6 to 10^7 Monte Carlo steps (MCS) before performing the averaging. The thermal average for a sample are taken from 2×10^7 to 3×10^8 MCS, and the larger the N or κ or c, the more the MCS. This is because the thermal fluctuation becomes larger with increasing N or κ or c. Moreover, we take $N = 20, 50, 100, 150, 200, 250, 300$ to examine the finite size effect. $c = 0.1, 0.2, 0.3, 0.4, 0.5$ and $\kappa = 1, 2, 4, 6, 8$ in most cases. However, for $c = 0.1$, we also take $\kappa = 15, 20, 25$ in the off-lattice system. We do not consider a larger c because it is impractical. We also do not consider a larger κ because it results in a very large fluctuation. This should result from the existence of metastable states (i.e., the states with a local minimum energy), since a larger bending rigidity can result in a higher energy barrier between different states and it follows that the system may be trapped longer in a metastable state.

The thermodynamical limit in this work means that we keep both l_0 and c as constants but let $N \to \infty$ so that the total length $L = Nl_0 \to \infty$. With such a convention, at the same c, a larger N gives a larger n_0 or more loops. Note that, to compare the results at $T > 0$ with the results at $T = 0$ exactly, one should decrease l_0 gradually but keep k, F_x, $\tilde{c}$, and L constant. However, such a procedure needs much more computational effort and clearly it does not correspond to a real system. We also do not expect that it can provide new insights into the mechanical property of the filament, so that we do not perform it in this work.

At a finite temperature, the fluctuation can suppress sharp transition, especially for a finite-size system. Therefore, to examine the occurrence of phase transition and to identify the nature of transition, one often has to evaluate the finite size effects. For this purpose, we study the specific heat $\mathcal{C}_N$, the stretching strength μ_N, and the fourth-order cumulants of the order parameter (U_N) and energy (V_N).[25] They are expressed as

$$\mathcal{C}_N \equiv \frac{\langle \mathcal{E}_N^2 \rangle - \langle \mathcal{E}_N \rangle^2}{N} \propto \frac{1}{N}\frac{\partial \langle E \rangle}{\partial T}, \tag{8}$$

$$\mu_N \equiv \frac{1}{N}\frac{\partial \langle x_N \rangle}{\partial f} = \frac{\langle x_N^2 \rangle - \langle x_N \rangle^2}{N}, \tag{9}$$

$$U_N \equiv 1 - \frac{\langle x_N^4 \rangle}{3\langle x_N^2 \rangle^2}, \quad V_N \equiv 1 - \frac{\langle \mathcal{E}_N^4 \rangle}{3\langle \mathcal{E}_N^2 \rangle^2}. \tag{10}$$

It has been reported that, for the first-order transition, V_N has a minimum at the effective transition point $f = f_N^*$ and $V_N \neq 2/3$ at the transition point $f = f^*$ as $N \to \infty$.[25] However, by scaling analysis, it is found that, for higher-order transitions, $V_N \to 2/3$ as $N \to \infty$ even at f^*.[25] Meanwhile, for sufficient large N, curves for U_N cross as a function of f at the "fixed point" value U^* and the location of the crossing "fixed point" gives a critical point. Moreover, by scaling analysis, when $N \to \infty$, $U_N \to 2/3$ if $f > f^*$, and $U_N \to 0$ if $f < f^*$; at f^*, U_N tends towards a universal value.

4.1 *Results of lattice system*

We have presented a brief report for the discrete model on the triangle and square lattice systems.[26] The main reason for

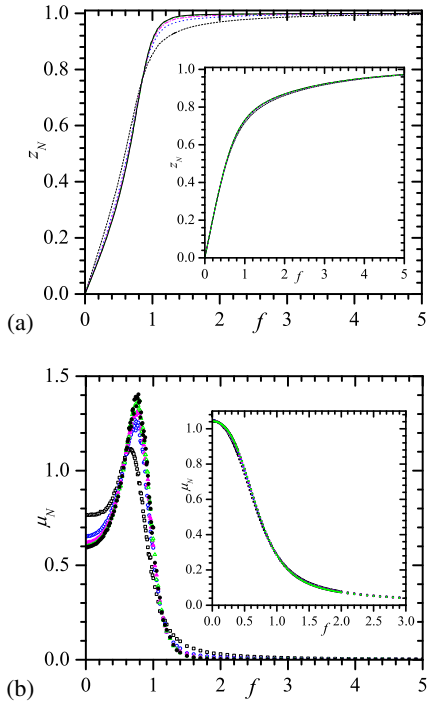

Fig. 5. (Color online) (a) z_N vs f for triangle lattice when $\kappa = 6$, $c = 0.5$ and $\kappa = 1$, $c = 0.5$ (inset). The lengths are $N = 20$ (black short-dashed), 50 (blue dotted), 100 (magenta dash-dotted), 200 (green dashed), and 300 (black solid). (b) μ_N vs f for triangle lattice when $\kappa = 6$, $c = 0.5$ and $\kappa = 1$, $c = 0.5$ (inset). The lengths are $N = 20$ (black empty-square), 50 (blue empty-circle), 100 (magenta filled-triangle), 200 (green empty-triangle), and 300 (black filled-circle). Reduced units are used.

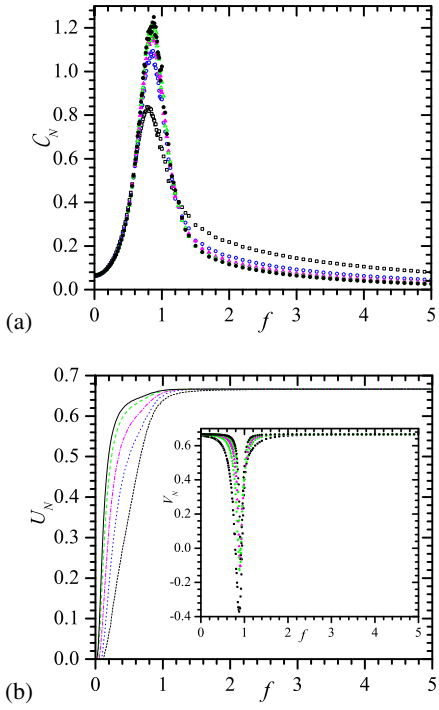

Fig. 6. (Color online) (a) C_N vs f for triangle lattice when $\kappa = 6$ and $c = 0.5$. (b) U_N and V_N (inset) vs f for triangle lattice when $\kappa = 6$ and $c = 0.5$. The symbols are the same as those in Fig. 5. Reduced units are used.

carrying out simulation in lattice systems is that there are energy gaps in these systems, so that intuitionally a small c ($<\pi/6$ for a triangle lattice and $<\pi/4$ for a square lattice) would favor a smooth varying of z_N because the GSC is always a straight line regardless of f; however, a large c would favor a discontinuous transition[26] because clearly the GSC is f-dependent. Therefore, if phase transition still occurs at a small c, we expect that the same transition occurs in the off-lattice system. For completeness and comparison, we present here the main conclusions in the lattice systems but with examples different from those in Ref. 26.

When both κ and c are small, we find that z_N increases monotonically with increasing f, but μ_N decreases monotonically with increasing f, as shown in the insets in Fig. 5 for a typical result with $\kappa = 1$ and $c = 0.5$. Therefore, there is no phase transition in these cases. However, when $\kappa > 4$ and $c \geq 0.2$, we find that μ_N has a sharp peak at some $f = f_N^*$ values, and that the height of the peak increases with increasing N. A typical sample with $\kappa = 6$ and $c = 0.5$ is shown in Fig. 5. We also find that C_N has a similar behavior to μ_N, as shown in Fig. 6(a). The sharp peaks in C_N and μ_N indicate the existence of phase transition in the thermodynamical limit.

As shown in the inset of Fig. 6(b), we find that in our simulations, $V_N \sim 2/3$ for a small f or a large f, but that V_N has a minimum at $<2/3$ at a moderate f. Meanwhile, in all the cases, we do not find any intersection point in U_N, and $U_N \to 2/3$ only when f is rather large, as shown in Fig. 6(b). These results suggest that phase transition is of the first-order.

Finally, note that all conclusions in this subsection are valid in both triangle and square lattice systems.

4.2 *Results in off-lattice system*

In lattice systems, we do not find discontinuous transition when L is finite or κ is small, so the results are quite different from those at $T = 0$. As discussed in Ref. 24, when c is small, the off-lattice system might favor a transition so that the results in the off-lattice system might be different from that in the lattice system. We should also remind everyone that the 2D lattice system is very difficult to realize in the experiment. Therefore, we also perform simulation in the off-lattice system.

In the off-lattice system, firstly, as shown in Fig. 7, under a low force, we find that at a large N the relationship between z_N and f approximately obeys $z_N = 2f\kappa/(1 + 4c^2\kappa^2)$ (dash-dot-dotted lines) which comes from the analytical analysis for the continuous model,[16] and the larger the N, the better the agreement. This result provides a robust proof of the accuracy of the simulation results, particularly of the irrelevance of the initial configurations. We should point out that the results in the lattice systems do not follow such a relation so that it is indeed necessary to study the off-lattice system.

However, qualitatively, we obtain the same conclusions as those for the lattice system.

Firstly, when both κ and c are small, we find that z_N increases monotonically with increasing f, but μ_N decreases monotonically with increasing f, as shown in the insets of Figs. 7(a) and 8(a) for a typical sample with $\kappa = 2$ and $c = 0.2$. Therefore, there is no phase transition in these cases. However, at a large κ and a large c, we find that there is a turning point in the $z_N - f$ relation so that μ_N and C_N have

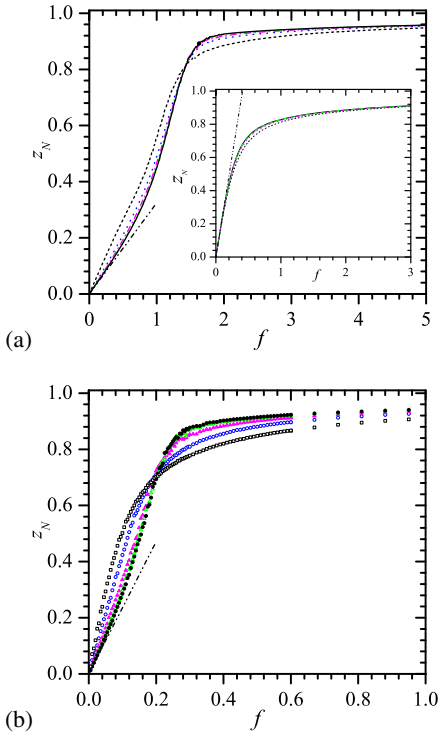

Fig. 7. (Color online) (a) z_N vs f for off-lattice system when $\kappa = 6$, $c = 0.5$ and $\kappa = 2$, $c = 0.2$ (inset). (b) z_N vs f for off-lattice system when $\kappa = 20$, $c = 0.1$. The dash-dot-dotted straight lines are given by $z_N = 2f\kappa/(1 + 4c^2\kappa^2)$, all the other symbols are the same as those in Fig. 5. Reduced units are used.

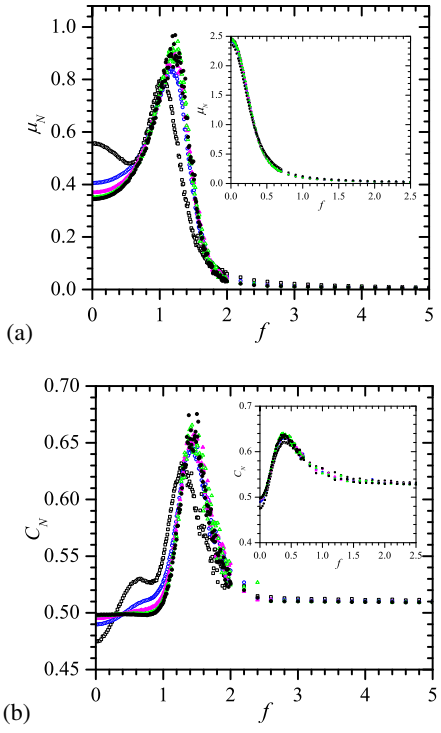

Fig. 8. (Color online) (a) μ_N vs f plots for off-lattice when $\kappa = 6$, $c = 0.5$ and $\kappa = 2$, $c = 0.2$ (inset). (b) $\mathcal{C}_N$ vs f plots for off-lattice system when $\kappa = 6$, $c = 0.5$ and $\kappa = 2$, $c = 0.2$ (inset). The symbols are the same as those in Fig. 5. Reduced units are used.

sharp peaks at some $f = f_N^*$, and the height of the peak increases with increasing N. Meanwhile, the larger the N, the sharper the peak. Two typical examples with $\kappa = 6$, $c = 0.5$ and $\kappa = 20$, $c = 0.1$ are shown in Figs. 7 and 8, respectively. Note that $\kappa \geq 20$ is not a too large value for a semiflexible biopolymer. For instance, if $l_0 \approx 1$ nm, for a dsDNA $\kappa \approx 50$. The growing sharp peaks in $\mathcal{C}_N$ and μ_N again indicate the existence of phase transition in the thermodynamical limit. Moreover, the unique peak at a large N in μ_N and $\mathcal{C}_N$ means that the transition is a single step instead of multiple steps occurring at $T = 0$. It is reasonable to surmise that this unique transition corresponds to the last step of transition at $T = 0$ since it can open several loops almost simultaneously, resulting in more than 30% changes in z_L. However, owing to the very strong fluctuations up to a rather large force, we cannot verify this conjecture by examining the changes in the instantaneous configuration directly by simulation. However, the fact that fluctuations eliminate the transition at a small c and a small κ supports the conjecture since, in this case, the energy differences between nearby configurations are small so that GSC cannot dominate the configurational average. Consequently, thermal average will remove all sharp jumps in z_N if κ is small, but can leave the largest jump if κ is large. Meanwhile, we have to point out that $\mathcal{C}_N$ always has a peak even when both c and κ are small, as shown in the inset of Fig. 8(b). However, the height of peak of $\mathcal{C}_N$ stops increasing at a large N so it does not correspond to any transition. This also suggests that, to analyze phase transition in extension, it is more reliable and useful to study μ_N than to study $\mathcal{C}_N$.

Secondly, at the same κ, we find that a larger c results in a larger f^* and that the height of the peak of μ_N, $\mu_N(f^*)$, decreases with increasing c, but that the ratio $\mu_N(f^*)/\mu_N(0)$ increases with increasing c, as shown in Fig. 9(a). Meanwhile, at the same c, we find that a larger κ leads to a larger f^*, $\mu_N(f^*)$ and $\mu_N(f^*)/\mu_N(0)$, as shown in Fig. 9(b).

Thirdly, as shown in the inset of Fig. 10(a), we find that $V_N \sim 2/3$ for a small f or a large f, but has a minimum with $V_N < 2/3$ at a moderate f. Moreover, when $n > 20$, we do not find any intersection point in U_N and $U_N \to 2/3$ only when f is rather large, as shown in Fig. 10(a). These results again suggest that phase transition should be of the first order. This is not surprising since, at $T = 0$, there is also a first-order transition.

Fourthly, we do not find a discontinuous transition at a finite length regardless of c or κ, quite different from that at $T = 0$. Note that, when $N = 300$, $c = 0.5$ corresponds to $n_0 = 23$ and $c = 0.1$ corresponds to $n_0 = 4$; at $T = 0$, there are multiple step discontinuous transitions when $n_0 \geq 1$. This means that the fluctuation strongly suppresses a sharp transition. However, we need to point out that we do not completely exclude the possibility of a discontinuous transition at a finite length if κ is very large, since at a very large κ the GSC will dominate the average and at $T = 0$ the last step of transition can result in more than 30% changes in z_L. We also have to point out that a large κ results in a large fluctuation and may make numerical calculations unstable so we do not use a very large κ in this work.

Fifthly, we also observe that the peaks of μ_N and $\mathcal{C}_N$ clearly do not appear at the same f up to $N = 300$, but they approach each other slowly with increasing N. This indicates that it is caused by the finite size effect and suggests that the finite size effect is very strong in the model.

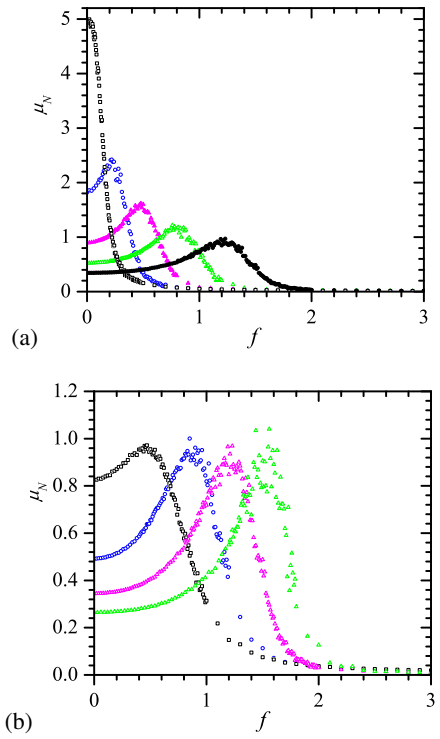

Fig. 9. (Color online) (a) μ_N vs f for off-lattice system when $N = 300$ and $\kappa = 6$, $c = 0.1$ (black empty-square), 0.2 (blue empty-circle), 0.3 (magenta filled-triangle), 0.4 (green empty-triangle), and 0.5 (black filled-circle). (b) μ_N vs f for off-lattice system when $N = 300$ and $c = 0.5$, $\kappa = 2$ (black empty-square), 4 (blue empty-circle), 6 (magenta filled-triangle), and 8 (green empty-triangle). Reduced units are used.

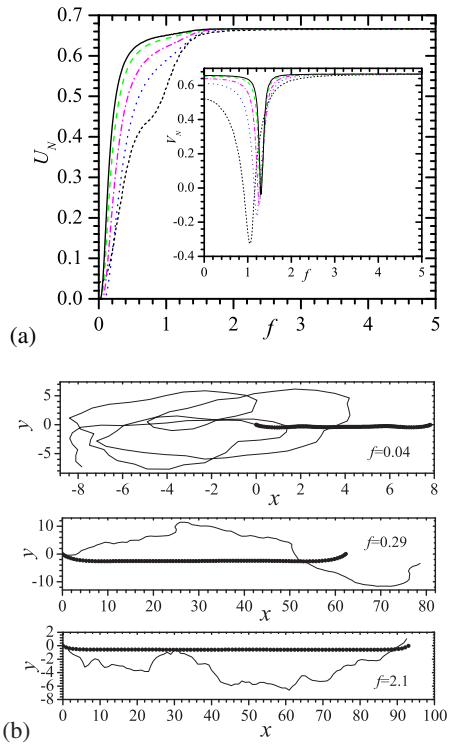

Fig. 10. (Color online) (a) U_N and V_N (inset) vs f for off-lattice system when $\kappa = 6$ and $c = 0.5$. The symbols are the same as those in Fig. 5. (b) Mean (filled circle) and instantaneous (solid line) configurations before and after transition for off-lattice system when $\kappa = 6$, $c = 0.2$, $N = 100$, and $f = 0.04$ (top), 0.29 (middle), and 2.1 (bottom). Reduced units are used.

Figure 10(b) shows some mean and instantaneous configurations before and after transition when $\kappa = 6$, $c = 0.2$, and $N = 100$ so $n_0 = 3$. From Fig. 10(b), we can see that before transition ($f = 0.04$) there are several loops, but after transition ($f = 0.29$ and 2.1) there is no longer a loop, so that the transition is indeed associated with unwinding loops. In fact, n can be greater than n_0 at $T > 0$ since entropy favors the formation of loops. For instance, the instantaneous configuration in the top panel of Fig. 10(b) ($f = 0.04$) has $n = 4 > n_0 = 3$. We also see that the mean configurations are highly symmetric, as it should be since we use hinged BC in simulation. We further find that the most instantaneous configurations are far from its mean configuration even when f is large, and that there may have no loop for the mean configurations even before transition. These results again indicate that the fluctuations in the system are very strong.

The above conclusions are valid in both lattice and off-lattice systems. However, there are still some differences between the two systems aside from the difference in behaviors in the low-force regime mentioned in the second paragraph of this subsection.

Firstly, we find that with the same N, κ, and c, f^* in the off-lattice system is always larger than that in the lattice system, as we can see by comparing Figs. 5 and 6 with Figs. 7 and 8. Moreover, the peaks for μ and $\mathcal{C}_N$ in the lattice system are always sharper than that in the off-lattice system. Therefore, the lattice structure favors a sharp transition even if c is small. This seems to be inconsistent with the intuitional conjecture that energy gaps in the lattice system would disfavor a sharp transition when c is small, since in this case the GSC is always a straight line regardless of force.[26] We can reconcile this apparent disagreement by noting that phase transition is dominated by unwinding loops instead of by the existence of an energy gap, so that an energy gap is not necessary for phase transition but that it accelerates the collapse of configurations into GSC and makes the transition sharper.

5. Conclusions and Discussion

In summary, we find that a nonvanishing intrinsic curvature can induce a discontinuous change in extension for a semiflexible biopolymer. The critical force increases with increasing intrinsic curvature or bending rigidity. At zero temperature, the transition is a multiple-step transition and accompanied by unwinding loops, regardless of the bending rigidity and length. However, a finite temperature represses the transition so that the discontinuous transition becomes an one-step transition, requires sufficient large intrinsic curvature and bending rigidity, and probably occurs only in the thermodynamical limit. These conclusions are valid in both lattice and off-lattice systems.

In the present work, we focus on the 2D system but we expect that it should be possible to observe similar phenomena in some constrained systems, such as in a flat box. Our results also suggest that a nonvanishing intrinsic curvature can play crucial role in determining the property of a filament in a crowded biological system, such as inside a cell. We should remind everyone that it is difficult to realize an ideal 2D system, so that for comparison with results of an experiment it may be better to study a 3D system. At zero

temperature, we expect that the conclusions must be the same in both 2D and 3D systems, because under uniaxial force and with hinged BC, the GSC in 3D space must also lie in a plane owing to symmetry, so that the results are the same as those in 2D space. However, we should also point out that this conclusion is correct only for a twist-free filament at zero temperature. In the 3D system, besides a strong fluctuation, torsional elasticity is important and mechanical properties will sensitively depend on the topological constraint and the twist conditions imposed at two ends.[5–9] Therefore, the applicability of the results in this work to a 3D system deserves a further study.

Acknowledgment

This work has been supported by the NSC, NCTS of the Republic of China.

Appendix: Derivation of Eqs. (5)–(7)

In this Appendix, we present the derivation of Eqs. (5)–(7). From Eq. (3), we find[16]

$$\dot{\phi}(s) = \pm|\tilde{c}|G(\phi) \text{ or } ds = \pm d\phi(s)/|\tilde{c}|G(\phi), \qquad (A\cdot1)$$

where $G(\phi) \equiv \sqrt{1 + F(\cos\phi_L - \cos\phi)}$ and $F \equiv 2F_x/(k\tilde{c}^2)$. The equation requires $\cos\phi_L > 1 - 1/F$. When $\tilde{c} > 0$, we cannot choose a negative sign for $\dot{\phi}(s)$ because it cannot satisfy BC. From BC, we find that $\dot{\phi}(0) = \dot{\phi}(L)$ so Eq. (A·1) leads to $\cos\phi_0 = \cos\phi_L$. Therefore, $\phi_L = 2n\pi \pm \phi_0$, with n being an integer. Furthermore, the symmetry requires that $x(s) + s(L - s) = 2x(L/2)$ and $y(s) = y(L - s)$; it leads to $\dot{x}(s) = \dot{x}(L - s)$ and $\dot{y}(s) = -\dot{y}(L - s)$, i.e., $\cos[\phi(s)] = \cos[\phi(L - s)]$ and $\sin[\phi(s)] = -\sin[\phi(L - s)]$. It follows that $\sin[\phi(L/2)] = 0$ or $\phi(L/2) = n\pi$ as well as $\phi_L = 2n\pi - \phi_0$. From the symmetry, we can also let $0 > \phi_0 \geq -\pi$. This is because the configuration with $\pi > \phi_0 \geq 0$ can be obtained by rotating the filament (with $0 > \phi_0 \geq -\pi$) 180° around the x-axis. Therefore, $(2n + 1)\pi \geq \phi_L > 2n\pi$. Using $dx = \cos\phi\, ds$ and Eq. (A·1), we find

$$x_L = \frac{1}{\tilde{c}}\int_{\phi_0}^{\phi_L}\frac{\cos\phi\, d\phi}{G(\phi)} = \frac{2}{\tilde{c}}\int_{n\pi}^{\phi_L}\frac{\cos\phi\, d\phi}{G(\phi)}, \qquad (A\cdot2)$$

where n is the number of loops. ϕ_L is determined by

$$L = \frac{2}{\tilde{c}}\int_{n\pi}^{\phi_L}\frac{d\phi}{G(\phi)}. \qquad (A\cdot3)$$

In principle, we can evaluate Eqs. (A·2) and (A·3) directly to determine the relationship between x_L and F. However, in practice, it often causes numerical instability for a large L. Therefore, we separate the periodic parts in these two equations as below so that we can avoid problems of numerical instability. Letting $\phi_L = 2n\pi + \phi'_L$, we have $\phi'_L = -\phi_0$ and $\pi \geq \phi'_L > 0$. For an arbitrary integer m, it is straightforward to show that

$$\int_{2m\pi}^{2(m+1)\pi}\frac{d\phi}{G(\phi)} = \int_0^{2\pi}\frac{d\phi}{G(\phi)} = \int_0^{\pi}\frac{2d\phi}{G(\phi)}, \qquad (A\cdot4)$$

$$\int_{2m\pi}^{2(m+1)\pi}\frac{\cos\phi\, d\phi}{G(\phi)} = \int_0^{2\pi}\frac{\cos\phi\, d\phi}{G(\phi)} = \int_0^{\pi}\frac{2\cos\phi\, d\phi}{G(\phi)}. \qquad (A\cdot5)$$

It follows then that

$$L = \frac{2n}{\tilde{c}}\int_0^{\pi}\frac{d\phi}{G(\phi)} + \frac{2}{\tilde{c}}\int_0^{\phi'_L}\frac{d\phi}{G(\phi)}, \qquad (A\cdot6)$$

$$x_L = \frac{2n}{\tilde{c}}\int_0^{\pi}\frac{\cos\phi\, d\phi}{G(\phi)} + \frac{2}{\tilde{c}}\int_0^{\phi'_L}\frac{\cos\phi\, d\phi}{G(\phi)}, \qquad (A\cdot7)$$

$$\mathcal{E}_L \equiv E_L/k\tilde{c} = \frac{1}{2\tilde{c}}\int_0^L(\dot{\phi}^2 - 2\tilde{c}\dot{\phi})ds - \tilde{c}Fx_L/2$$
$$= n\int_0^{\pi}G(\phi)d\phi + \int_0^{\phi'_L}G(\phi)d\phi - 2(n\pi + \phi'_L) - \tilde{c}Fx_L/2, \qquad (A\cdot8)$$

where we have omitted the constant term in E_L. Equations (A·6)–(A·8) recover Eqs. (5)–(7), respectively.

*zzhou@mail.tku.edu.tw

1) J. F. Marko and E. D. Siggia, Science **265**, 506 (1994).
2) C. Bustamante, J. F. Marko, E. D. Siggia, and S. Smith, Science **265**, 1599 (1994).
3) J. F. Marko and E. D. Siggia, Macromolecules **28**, 8759 (1995).
4) B. Smith, Y. V. Zastavker, and G. B. Benedek, Phys. Rev. Lett. **87**, 278101 (2001).
5) D. A. Kessler and Y. Rabin, Phys. Rev. Lett. **90**, 024301 (2003).
6) Z. Zhou, P.-Y. Lai, and B. Joós, Phys. Rev. E **71**, 052801 (2005).
7) Z. Zhou, B. Joós, P.-Y. Lai, Y.-S. Young, and J.-H. Jan, Mod. Phys. Lett. B **21**, 1895 (2007).
8) H. Wada and R. R. Netz, Europhys. Lett. **77**, 68001 (2007).
9) E. L. Starostin and G. H. M. van der Heijden, Phys. Rev. Lett. **101**, 084301 (2008).
10) H. R. Drew and A. A. Travers, J. Mol. Biol. **186**, 773 (1985).
11) M. Dlakic, K. Park, J. D. Griffith, S. C. Harvey, and R. E. Harrington, J. Biol. Chem. **271**, 17911 (1996).
12) W. Han, S. M. Lindsay, M. Dlakic, and R. E. Harrington, Nature **386**, 563 (1997).
13) W. Han, M. Dlakic, Y. J. Zhu, S. M. Lindsay, and R. E. Harrington, Proc. Natl. Acad. Sci. U.S.A. **94**, 10565 (1997).
14) J. Moukhtar, E. Fontaine, C. Faivre-Moskalenko, and A. Arneodo, Phys. Rev. Lett. **98**, 178101 (2007).
15) C. Vaillant, B. Audit, and A. Arnéodo, Phys. Rev. Lett. **95**, 068101 (2005).
16) Z. Zhou, Phys. Rev. E **76**, 061913 (2007).
17) Z. Zhou and B. Joós, Phys. Rev. E **80**, 061911 (2009).
18) A. Arneodo, E. Bacry, P. V. Graves, and J. F. Muzy, Phys. Rev. Lett. **74**, 3293 (1995).
19) D. C. Schwartz, X. Li, L. I. Hernandez, S. P. Ramnarain, E. J. Huff, and Y. K. Wang, Science **262**, 110 (1993).
20) A. Prasad, Y. Hori, and J. Kondev, Phys. Rev. E **72**, 041918 (2005).
21) I. M. Kulić, H. Mohrbach, R. Thaokar, and H. Schiessel, Phys. Rev. E **75**, 011913 (2007).
22) B. Maier, U. Seifert, and J. O. Rädler, Europhys. Lett. **60**, 622 (2002).
23) D. Marenduzzo, A. Maritan, A. Rosa, and F. Seno, Phys. Rev. Lett. **90**, 088301 (2003).
24) A. Rosa, D. Marenduzzo, A. Maritan, and F. Seno, Phys. Rev. E **67**, 041802 (2003).
25) D. P. Landau and K. Binder, *A Guide to Monte Carlo Simulation in Statistical Physics* (Cambridge University Press, Cambridge, U.K., 2005) 2nd ed., Chap. 4, pp. 78 and 85.
26) Z. Zhou and F.-T. Lin, APPC12; to be published in JPS Conf. Proc. (2014).